

Low-rank tensor approximations for solving multi-marginal optimal transport problems

Christoph Strössner¹ and Daniel Kressner¹

¹Ecole Polytechnique Fédérale de Lausanne (EPFL), Institute of Mathematics, CH-1015 Lausanne, Switzerland

christoph.stroessner@epfl.ch, daniel.kressner@epfl.ch

February 16, 2022

Abstract

By adding entropic regularization, multi-marginal optimal transport problems can be transformed into tensor scaling problems, which can be solved numerically using the multi-marginal Sinkhorn algorithm. The main computational bottleneck of this algorithm is the repeated evaluation of marginals. In [Haasler et al., *IEEE Trans. Inf. Theory*, 67 (2021)], it has been suggested that this evaluation can be accelerated when the application features an underlying graphical model. In this work, we accelerate the computation further by combining the tensor network dual of the graphical model with additional low-rank approximations. For the color transfer of images, these added low rank approximations save more than 96% of the computation time.

1 Introduction

Classical optimal transport minimizes the transport cost between $m = 2$ probability measures [7, 46]. For discrete measures, this problem can be expressed as the minimization of $\langle C, P \rangle$ for a non-negative cost matrix C . The so called transport plan P is a non-negative matrix that has to satisfy marginal constraints, i.e., the column and row sums of P are prescribed. The pioneering work of Cuturi [14] established a relation between entropy regularized optimal transport and matrix scaling of $\exp(-C/\eta)$, where \exp denotes the elementwise exponential and $\eta > 0$ denotes the regularization parameter. Scaling the rows and columns of $\exp(-C/\eta)$ such that marginal constraints are satisfied can be achieved numerically using the Sinkhorn algorithm [44], whose convergence speed can be accelerated using greedy coordinate descent [2, 32], overrelaxation [45] or accelerated gradient descent [16]. This matrix scaling approach allows one to solve much larger optimal transport problems compared to previous attempts based on solving the original linear program, which in turn has impacted various fields including image processing [19, 39], data science [38], engineering [34] and machine learning [22, 30].

The classical optimal transport problem can be generalized to a multi-marginal setting, in which the transport cost between $m \geq 3$ measures is minimized [37]. Such multi-marginal problems arise in the areas of density functional theory [15], generalized incompressible flow [9], neural networks [10],

signal processing [17] and Wasserstein barycenters [12]. For discrete measures, the problem can be expressed as finding the non-negative transport plan tensor \mathcal{P} of order m which minimizes $\langle \mathcal{C}, \mathcal{P} \rangle$ subject to marginal constraints, where \mathcal{C} denotes a given non-negative cost tensor of order m . In analogy to the the matrix case, after adding entropic regularization the problem can equivalently be transformed into a tensor scaling problem for the tensor $\exp(-\mathcal{C}/\eta)$ [8]. The Sinkhorn algorithm can be generalized to solve this multi-marginal problem [11]; acceleration techniques via greedy coordinate descent are described in [21, 31].

The multi-marginal Sinkhorn algorithm crucially relies on the repeated evaluation of marginals of the rescaled tensor $\exp(-\mathcal{C}/\eta)$. The cost of computing such a marginal increases exponentially in m . However, under certain assumptions on the structure of $\exp(-\mathcal{C}/\eta)$, marginals can be computed much more efficiently. For instance, certain applications allow to specify $\exp(-\mathcal{C}/\eta)$ in terms of a graphical model. When this graphical model does not contain circles, marginals can be computed efficiently using the believe propagation algorithm [18, 25]. In particular, this includes tree structured cost tensors [6, 24]. Even when $\exp(-\mathcal{C}/\eta)$ cannot be specified exactly via a graphical model, it may still be possible to attain complexity reduction by performing a low-rank approximation defined by such a model. For the classical case $m = 2$, this corresponds to low-rank approximation of the matrix $\exp(-C/\eta)$ and Altschuler et al. [1] analyze the impact of the low-rank approximation error on the solution returned by the Sinkhorn algorithm. For the case $m \geq 3$, analogous error bounds for low-rank approximations of $\exp(-\mathcal{C}/\eta)$ are implicitly used in [3] to prove complexity bounds. These theoretical bounds exploit that $\exp(-\mathcal{C}/\eta)$ is approximately low-rank when \mathcal{C} has low tensor rank [28] and is given explicitly in factored form. The practical usefulness of these results is impeded by the fact that the elementwise exponential tends to increase (approximate) ranks drastically, for example to obtain a reasonably good approximation to the elementwise exponential of a large random rank-5 matrix one easily ends up with a matrix of rank 800 or larger. Let us point out that low-rank approximations of $\exp(-\mathcal{C}/\eta)$ should not be confused with low-rank approximations of the desired transport plan, as proposed in [43].

The main contribution of this work is to combine low-rank approximations and graphical models for $\exp(-\mathcal{C}/\eta)$ to compute marginals more efficiently. We propose to transform the graphical model into its dual tensor network [41]. Facilitating this point of view, we compute marginals of the rescaled tensor $\exp(-\mathcal{C}/\eta)$ by contracting [40] the tensor network and the scaling parameters. These contractions can be evaluated even if the graphical model contains circles. The computation of these contractions is accelerated further by replacing tensors and matrices contained in the tensor network by low-rank approximations. We analyze how these low-rank truncations affect the multi-marginal Sinkhorn algorithm. In particular, we generalize the result from [1] to tensors. As a special case, we obtain a bound on the error introduced by approximations in tensor networks. Moreover, we provide an example illustrating that our approach is more efficient than directly working with the graphical model and more accurate than a direct tensor train approximation [36] of $\exp(-\mathcal{C}/\eta)$. We also demonstrate that introducing low-rank approximations offers the potential to greatly speed up the computation of color transfer between several images without altering the resulting image significantly.

2 Multi-marginal optimal transport and the Sinkhorn algorithm

2.1 Mathematical setting

We let $\Delta^n = \{x \in \mathbb{R}_{>0}^n : \|x\|_1 = 1\}$ denote the set of strictly positive probability vectors of length n , where $\mathbb{R}_{>0}$ denotes the strictly positive real numbers and $\|\cdot\|_1$ denotes the ℓ^1 -norm. Let \mathbb{R}_+ denote the non-negative real numbers. For a tensor $\mathcal{X} \in \mathbb{R}_+^{n_1 \times \dots \times n_m}$ containing the joint probability distribution of m random variables, the k th marginal (distribution) is obtained by summing up over all but the k th index. Using the mode- k product \times_k , see [29], this operation can be expressed as

$$r_k(\mathcal{X}) = \mathcal{X} \times_1 \mathbf{1}_{n_1}^T \cdots \times_{k-1} \mathbf{1}_{n_{k-1}}^T \times_{k+1} \mathbf{1}_{n_{k+1}}^T \cdots \times_m \mathbf{1}_{n_m}^T,$$

where $\mathbf{1}_n \in \mathbb{R}^n$ denotes a vector of all ones.

Given $m \geq 2$ marginals $r_k \in \Delta^{n_k}$, $k = 1, \dots, m$ and a cost tensor $\mathcal{C} \in \mathbb{R}_+^{n_1 \times n_2 \times \dots \times n_m}$, the discrete multi-marginal optimal transport problem is given by

$$\min_{\mathcal{P} \in B(r_1, \dots, r_m)} \langle \mathcal{P}, \mathcal{C} \rangle, \quad (1)$$

where the set of feasible transport plans is given by

$$B(r_1, \dots, r_m) = \{\mathcal{P} \in \mathbb{R}_+^{n_1 \times \dots \times n_m} \text{ such that } r_k(\mathcal{P}) = r_k \text{ for } k = 1, \dots, m\}$$

and $\langle \cdot, \cdot \rangle$ denotes the standard inner product, that is,

$$\langle \mathcal{P}, \mathcal{C} \rangle = \sum_{i_1=1}^{n_1} \cdots \sum_{i_m=1}^{n_m} \mathcal{P}_{i_1, \dots, i_m} \mathcal{C}_{i_1, \dots, i_m}.$$

Note that (1) is a linear optimization problem with $n_1 \cdot n_2 \cdots n_m$ degrees of freedom.

To solve (1) efficiently, it is common to add entropic regularization [14]. In the multi-marginal setting, the entropy takes the form

$$H(\mathcal{P}) = -\langle \mathcal{P}, \log(\mathcal{P}) \rangle,$$

where \log is applied elementwise. Given a regularization parameter $\eta > 0$, the regularized problem takes the form

$$\min_{\mathcal{P} \in B(r_1, \dots, r_m)} V_{\mathcal{C}}^{\eta}(\mathcal{P}), \quad (2)$$

where

$$V_{\mathcal{C}}^{\eta}(\mathcal{P}) := \langle \mathcal{P}, \mathcal{C} \rangle - \eta H(\mathcal{P})$$

is called entropic transport cost. It is known that the regularized problem (2) has a unique minimizer [8], which takes the form

$$\mathcal{P}_{\eta}^* = \mathcal{K} \times_1 \text{diag}(\exp(\beta_1)) \cdots \times_m \text{diag}(\exp(\beta_m)), \quad (3)$$

where $\mathcal{K} := \exp(-\mathcal{C}/\eta)$ is called Gibbs kernel [11] and $\text{diag}(\beta_k)$ denotes the diagonal matrix containing the entries of the so called scaling parameters $\beta_k \in \mathbb{R}^{n_k}$ on its diagonal. The solution of the regularized problem (2) converges to a solution of (1) when $\eta \rightarrow 0$; see [38, Proposition 4.1].

2.2 Multi-marginal Sinkhorn algorithm

The multi-marginal Sinkhorn algorithm for solving (2) proceeds by iteratively updating the scaling parameters in (3). Let

$$\mathcal{P}_\eta^{(t)} = \mathcal{K} \times_1 \text{diag}(\exp(\beta_1^{(t)})) \cdots \times_m \text{diag}(\exp(\beta_m^{(t)})) \quad (4)$$

denote the scaled tensor obtained after t iterations. In each iteration one selects an index k and updates the k th vector of scaling parameters via $\beta_k^{(t+1)} = \log(r_k) - \log(r_k(\mathcal{P}_\eta^{(t)})) + \beta_k^{(t)}$, while the other vectors remain unchanged. For the choice of indices it has been suggested to traverse them cyclically [8] or use a greedy heuristics [21, 31]. The multi-marginal Sinkhorn algorithm is terminated once the stopping criterion

$$\sum_{k=1}^m \|r_k(\mathcal{P}_\eta^{(t)}) - r_k\|_1 \leq \varepsilon_{\text{stop}} \quad (5)$$

is satisfied, where $\varepsilon_{\text{stop}} > 0$ denotes a prescribed tolerance. Algorithm 1 summarizes the described procedure.

Algorithm 1 Multi-marginal Sinkhorn algorithm

- 1: **Input:** cost tensor \mathcal{C} , marginals r_1, \dots, r_m , regularization parameter η
 - 2: **Output:** transport plan $\mathcal{P}_\eta^{(t)}$
 - 3: $\beta_i^{(0)} = \mathbf{0} \in \mathbb{R}^{n_i}$ for $i = 1, \dots, m$ and $\mathcal{K} = \exp(-\mathcal{C}/\eta)$
 - 4: **for** $t = 0, 1, \dots$ until stopping criterion (5) is satisfied
 - 5: $\mathcal{P}_\eta^{(t)} = \mathcal{K} \times_1 \text{diag}(\exp(\beta_1^{(t)})) \cdots \times_m \text{diag}(\exp(\beta_m^{(t)}))$
 - 6: Let k_{next} denote the index of the scaling parameter, which should be updated next.
 - 7: $\beta_k^{(t+1)} = \begin{cases} \log(r_k) - \log(r_k(\mathcal{P}_\eta^{(t)})) + \beta_k^{(t)} & k = k_{\text{next}} \\ \beta_k^{(t)} & k \neq k_{\text{next}} \end{cases}$
-

When using cyclic order, it follows from an interpretation as Bregman projections [8] that the multi-marginal Sinkhorn algorithm converges. For greedy strategies, Theorem 1 below summarizes results from [21, 31], bounding the number of iterations until the stopping criterion is reached. Note that the bound in a) gives a better rate with respect to $\varepsilon_{\text{stop}}$, but the bound depends on r_k , whereas the bound in b) does not involve r_k .

Theorem 1. Let $\mathcal{C} \in \mathbb{R}_+^{n_1 \times \dots \times n_m}$, $r_k \in \Delta^{n_k}$ for $k = 1, \dots, m$, $0 < \eta < \frac{1}{2}$, and $\varepsilon_{\text{stop}} > 0$.

a) Suppose that Algorithm 1 selects the index of the scaling parameter in iteration t according to

$$k_{\text{next}} = \arg \max_{k \in \{1, \dots, m\}} \|r_k(\mathcal{P}_\eta^{(t)}) - r_k\|_1 + \|r_k \circ \log(r_k(\mathcal{P}_\eta^{(t)})) \circ r_k^{-1}\|_1,$$

where \circ and r_k^{-1} denote the elementwise product and elementwise inverse, respectively. Then the number of iterations to reach the stopping criterion (5) is bounded by

$$t \leq 2 + 2m^2 \varepsilon_{\text{stop}}^{-1} (\eta^{-1} \|\mathcal{C}\|_\infty - \log \min_{1 \leq k \leq m} \min_{1 \leq i \leq n_k} (r_k)_i), \quad (6)$$

where $\|\cdot\|_\infty$ denotes the uniform norm.

b) Assume that $n = n_1 = \dots = n_m$ and suppose that Algorithm 1 normalizes $\mathcal{P}_\eta^{(0)}$ to have ℓ^1 -norm 1 and selects the index of the scaling parameter in iteration t according to

$$k_{\text{next}} = \arg \max_{k \in \{1, \dots, m\}} \left\| r_k(\mathcal{P}_\eta^{(t)}) - \frac{\langle r_k, r_k(\mathcal{P}_\eta^{(t)}) \rangle}{\|r_k\|_2^2} r_k \right\|_1. \quad (7)$$

Then the number of iterations needed to reach the stopping criterion

$$\max_{k \in \{1, \dots, m\}} \left\| r_k(\mathcal{P}_\eta^{(t)}) - \frac{\langle r_k, r_k(\mathcal{P}_\eta^{(t)}) \rangle}{\|r_k\|_2^2} r_k \right\|_1 < \frac{\varepsilon_{\text{stop}}}{2m} \quad (8)$$

is bounded by

$$t \leq 4m^2(\sqrt{n} + 1)^2 \varepsilon_{\text{stop}}^{-2} \log(\eta^{-1} \|\exp(-\mathcal{C}/\eta)\|_1).$$

When the alternative stopping criterion (8) is satisfied, the stopping criterion (5) is also satisfied.

Proof. Part a) follows from Theorem 4.3 in [31]. Part b) follows from Theorem 3.4 and Lemma B.1 in [21]. \square

A transport plan $\hat{\mathcal{P}} \in B(r_1, \dots, r_m)$ is called ε -approximate solution of the original problem (1) if it satisfies

$$\langle C, \hat{\mathcal{P}} \rangle \leq \min_{\mathcal{P} \in B(r_1, \dots, r_m)} \langle C, \mathcal{P} \rangle + \varepsilon.$$

The transport plan $\mathcal{P}_\eta^{(t)}$ obtained from Algorithm 1 using either stopping criterion from Theorem 1 is, in general, not in $B(r_1, \dots, r_m)$ because the marginal constraints $r_k = r_k(\mathcal{P}_\varepsilon^{(t)})$ are satisfied simultaneously only in the limit $t \rightarrow \infty$. To fix this issue, rounding [2] can be applied to enforce the marginal constraints on $\mathcal{P}_\varepsilon^{(t)}$ for finite t ; see Algorithm 2. Note that for a tensor of the form (4), the operation in line 5 of Algorithm 2 can be phrased in terms of modifying $\beta_k^{(t)}$. Line 6 is a rank-1 update. In [21, Lemma 3.6] and in [31, Theorem 4.4], the following property of the resulting tensor is proven.

Lemma 1. Let $\mathcal{A} \in \mathbb{R}_{>0}^{n_1 \times \dots \times n_m}$ and $r_k \in \Delta^{n_k}$, $k = 1, \dots, m$. Let \mathcal{B} denote the output of Algorithm 2 applied to \mathcal{A} and r_1, \dots, r_m . Then $\mathcal{B} \in B(r_1, \dots, r_m)$ and

$$\|\mathcal{A} - \mathcal{B}\|_1 \leq 2 \sum_{k=1}^m \|r_k - r_k(\mathcal{A})\|_1.$$

Algorithm 2 Rounding

- 1: **Input:** tensor $\mathcal{A} \in \mathbb{R}_{>0}^{n_1 \times \dots \times n_m}$, vectors $r_k \in \Delta^{n_k}$ for $k = 1, \dots, m$
 - 2: **Output:** tensor $\mathcal{B} \in \mathbb{R}^{n_1 \times \dots \times n_m}$
 - 3: **for** $k = 1, \dots, m$
 - 4: $v = \min(r_k(\mathcal{A})^{-1} \circ r_k, \mathbf{1}_{n_k})$, where the min is taken elementwise
 - 5: $\mathcal{A} = \mathcal{A} \times_k \text{diag}(v)$
 - 6: $\mathcal{B} = \mathcal{A} + \|r_1 - r_1(\mathcal{A})\|_1^{-(m-1)} \bigotimes_{k=1}^m (r_k - r_k(\mathcal{A}))$, where \bigotimes denotes the outer product, see [29]
-

Combining Algorithm 2 with Algorithm 1, using the index selection (7) and the stopping criterion (5), it follows [21, Corollary 3.8] that an ε -approximate solution can be computed in

$$\mathcal{O}(\varepsilon^{-3} m^4 n^{m+1} \log(n) (\max(\mathcal{C}) - \min(\mathcal{C}))^3)$$

operations, where $n_1 = \dots = n_K = n$. In practice, the computation can be accelerated by using slightly modified marginals and tolerances in the Sinkhorn algorithm [31], which ensure that the upper bound (6) for t is not dominated by small entries in r_k .

3 Impact of approximating the Gibbs kernel

To accelerate the computation of marginals in the multi-marginal Sinkhorn algorithm, we will replace the Gibbs kernel \mathcal{K} by an approximation $\tilde{\mathcal{K}}$; thus replacing Algorithm 1 by Algorithm 3. In this section, we will analyze the impact of this approximation on the transport plan. For $m = 2$, such an analysis can be found in [1, Theorem 5]. A generalization of this theorem to $m \geq 3$ is implicitly used in the proof of Theorem 5.3 in [3] but not stated explicitly. In the following, we derive this generalization in detail along with explicit constants, which are not stated in [1].

Algorithm 3 Multi-marginal Sinkhorn algorithm for a Gibbs kernel approximation

- 1: **Input:** approximation $\tilde{\mathcal{K}} \in \mathbb{R}_{>0}^{n_1 \times n_2 \cdots \times n_m}$ of Gibbs kernel $\mathcal{K} = \exp(-\mathcal{C}/\eta)$, marginals r_1, \dots, r_m
 - 2: **Output:** transport plan $\tilde{\mathcal{P}}^{(t)}$
 - 3: $\beta_i^{(0)} = \mathbf{0} \in \mathbb{R}^{n_i}$ for $i = 1, \dots, m$
 - 4: **for** $t = 0, 1, \dots$ until stopping criterion is reached
 - 5: $\tilde{\mathcal{P}}^{(t)} = \tilde{\mathcal{K}} \times_1 \text{diag}(\exp(\beta_1^{(t)})) \cdots \times_m \text{diag}(\exp(\beta_m^{(t)}))$
 - 6: Let k_{next} denote the index of the scaling parameter, which should be updated next.
 - 7: $\beta_k^{(t+1)} = \begin{cases} \log(r_k) - \log(r_k(\tilde{\mathcal{P}}^{(t)})) + \beta_k^{(t)} & k = k_{\text{next}} \\ \beta_k^{(t)} & k \neq k_{\text{next}} \end{cases}$
-

Theorem 2. Let $\mathcal{K} = \exp(-\mathcal{C}/\eta)$ and assume that $\tilde{\mathcal{K}} \in \mathbb{R}_{>0}^{n_1 \times n_2 \cdots \times n_m}$ with $n_i \geq 2$ and $m \geq 2$, satisfies

$$\|\log(\mathcal{K}) - \log(\tilde{\mathcal{K}})\|_\infty \leq \varepsilon_{\log} \leq 1.$$

Let $\tilde{\mathcal{P}}$ denote the transport plan returned by Algorithm 3 with stopping criterion $\sum_{k=1}^m \|r_k(\tilde{\mathcal{P}}) - r_k\|_1 \leq \varepsilon_{\text{stop}}$. Then

$$|V_{\mathcal{C}}^\eta(\mathcal{P}_\eta^*) - V_{\mathcal{C}}^\eta(\tilde{\mathcal{P}})| \leq \varepsilon_{V_{\mathcal{C}}^\eta}, \quad (9)$$

where $\mathcal{P}_\eta^* = \min_{\mathcal{P} \in B(r_1, \dots, r_m)} V_{\mathcal{C}}^\eta(\mathcal{P})$ and

$$\begin{aligned} \varepsilon_{V_{\mathcal{C}}^\eta} = & \eta \left(\varepsilon_{\log} \left(2 + \log \left(\frac{2}{\varepsilon_{\log}} \right) \right) + \frac{\varepsilon_{\log}}{2} \log \left(\left(\prod_{k=1}^m n_k \right) - 1 \right) + 2\varepsilon_{\text{stop}} \log \left(\frac{1}{\varepsilon_{\text{stop}}} \left(\left(\prod_{k=1}^m n_k \right) - 1 \right) \right) \right) \\ & + (\varepsilon_{\log} + 2\varepsilon_{\text{stop}}) \|\mathcal{C}\|_\infty. \end{aligned} \quad (10)$$

Proof. We denote by Π^S the operator mapping a given tensor $\mathcal{T} \in \mathbb{R}_{>0}^{n_1 \times \cdots \times n_m}$ to its unique [20] tensor scaling $\mathcal{U} \in B(r_1, \dots, r_m)$ of the form $\mathcal{U} = \mathcal{T} \times_1 \text{diag}(\gamma_1) \times_2 \cdots \times_m \text{diag}(\gamma_m)$ for some vectors

$\gamma_k \in \mathbb{R}_{>0}^{n_k}$ for $1 \leq k \leq m$. Observe that $\mathcal{P}_\eta^* = \Pi^S(\mathcal{K})$. Using the triangle inequality, we decompose the error into

$$|V_{\mathcal{C}}^\eta(\mathcal{P}_\eta^*) - V_{\tilde{\mathcal{C}}}^\eta(\tilde{\mathcal{P}})| \leq |V_{\mathcal{C}}^\eta(\Pi^S(\mathcal{K})) - V_{\mathcal{C}}^\eta(\Pi^S(\tilde{\mathcal{K}}))| \quad (11)$$

$$+ |V_{\mathcal{C}}^\eta(\Pi^S(\tilde{\mathcal{K}})) - V_{\tilde{\mathcal{C}}}^\eta(\Pi^S(\tilde{\mathcal{K}}))| \quad (12)$$

$$+ |V_{\tilde{\mathcal{C}}}^\eta(\Pi^S(\tilde{\mathcal{K}})) - V_{\tilde{\mathcal{C}}}^\eta(\tilde{\mathcal{P}})| \quad (13)$$

$$+ |V_{\tilde{\mathcal{C}}}^\eta(\tilde{\mathcal{P}}) - V_{\mathcal{C}}^\eta(\tilde{\mathcal{P}})| \quad (14)$$

where $\tilde{\mathcal{C}} = -\eta \log(\tilde{K})$. We derive bounds for each of these terms; their combination yields inequality (10).

Bound for (11): By definition of $V_{\mathcal{C}}^\eta$, we have

$$|V_{\mathcal{C}}^\eta(\Pi^S(\mathcal{K})) - V_{\mathcal{C}}^\eta(\Pi^S(\tilde{\mathcal{K}}))| \leq \|\Pi^S(\mathcal{K}) - \Pi^S(\tilde{\mathcal{K}})\|_1 \|\mathcal{C}\|_\infty + \eta |H(\Pi^S(\mathcal{K})) - H(\Pi^S(\tilde{\mathcal{K}}))|.$$

Because of $\arg \min_{\mathcal{P} \in B(r_1, \dots, r_m)} V_{\mathcal{C}}^\eta(\mathcal{P}) = \arg \min_{\mathcal{P} \in B(r_1, \dots, r_m)} \langle -\log(\mathcal{K}), \mathcal{P} \rangle - H(\mathcal{P})$, it follows that

$$\|\Pi^S(\mathcal{K}) - \Pi^S(\tilde{\mathcal{K}})\|_1 = \left\| \arg \min_{\mathcal{P} \in B(r_1, \dots, r_m)} \langle -\log(\mathcal{K}), \mathcal{P} \rangle - H(\mathcal{P}) - \left(\arg \min_{\tilde{\mathcal{P}} \in B(r_1, \dots, r_m)} \langle -\log(\tilde{\mathcal{K}}), \tilde{\mathcal{P}} \rangle - H(\tilde{\mathcal{P}}) \right) \right\|_1.$$

Applying Lemma I in [1] to the right hand side of this expression yields $\|\Pi^S(\mathcal{K}) - \Pi^S(\tilde{\mathcal{K}})\|_1 \leq \|\log \mathcal{K} - \log \tilde{\mathcal{K}}\|_\infty \leq \varepsilon_{\log}$. From Theorem 6 in [27] and Lemma D in [1] we obtain

$$|H(\Pi^S(\mathcal{K})) - H(\Pi^S(\tilde{\mathcal{K}}))| \leq \varepsilon_{\log} \log \left(\frac{2}{\varepsilon_{\log}} \right) + \frac{\varepsilon_{\log}}{2} \log \left(\left(\prod_{k=1}^m n_k \right) - 1 \right).$$

Bound for (12) and (14): Using that $\|\Pi^S(\tilde{\mathcal{K}})\|_1 = \|\tilde{\mathcal{P}}\|_1 = 1$ we obtain

$$|V_{\mathcal{C}}^\eta(\Pi^S(\tilde{\mathcal{K}})) - V_{\tilde{\mathcal{C}}}^\eta(\Pi^S(\tilde{\mathcal{K}}))| \leq \langle \mathcal{C}, \Pi^S(\tilde{\mathcal{K}}) \rangle - \langle \tilde{\mathcal{C}}, \Pi^S(\tilde{\mathcal{K}}) \rangle \leq \|\mathcal{C} - \tilde{\mathcal{C}}\|_\infty \leq \eta \varepsilon_{\log},$$

$$|V_{\tilde{\mathcal{C}}}^\eta(\tilde{\mathcal{P}}) - V_{\mathcal{C}}^\eta(\tilde{\mathcal{P}})| \leq \langle \mathcal{C}, \tilde{\mathcal{P}} \rangle - \langle \tilde{\mathcal{C}}, \tilde{\mathcal{P}} \rangle \leq \|\mathcal{C} - \tilde{\mathcal{C}}\|_\infty \leq \eta \varepsilon_{\log}.$$

Bound for (13): Using that the tensor $\tilde{\mathcal{P}}$ is the unique minimizer of $\arg \min_{\mathcal{P} \in B(r_1(\tilde{\mathcal{P}}), \dots, r_m(\tilde{\mathcal{P}}))} V_{\tilde{\mathcal{C}}}^\eta(\mathcal{P})$,

Lemma H in [1] yields

$$|V_{\tilde{\mathcal{C}}}^\eta(\Pi^S(\tilde{\mathcal{K}})) - V_{\tilde{\mathcal{C}}}^\eta(\tilde{\mathcal{P}})| \leq \omega(d_H(B(r_1(\tilde{\mathcal{P}}), \dots, r_m(\tilde{\mathcal{P}})), B(r_1, \dots, r_m))),$$

where $d_H(\cdot, \cdot)$ denotes the Hausdorff distance and

$$\omega(x) = x \|\mathcal{C}\|_\infty + \eta \left(x \log \left(\frac{2}{x} \left(\left(\prod_{k=1}^m n_k \right) - 1 \right) \right) \right).$$

We can bound $d_H(B(r_1(\tilde{\mathcal{P}}), \dots, r_m(\tilde{\mathcal{P}})), B(r_1, \dots, r_m))$ by $2\varepsilon_{\text{stop}}$, since Algorithm 2 maps any $\mathcal{A} \in B(r_1(\tilde{\mathcal{P}}), \dots, r_m(\tilde{\mathcal{P}}))$ to $\mathcal{B} \in B(r_1, \dots, r_m)$ with $\|\mathcal{A} - \mathcal{B}\|_1 \leq 2\varepsilon_{\text{stop}}$ as stated in Lemma 1. This implies

$$|V_{\tilde{\mathcal{C}}}^\eta(\Pi^S(\tilde{\mathcal{K}})) - V_{\tilde{\mathcal{C}}}^\eta(\tilde{\mathcal{P}})| \leq 2\varepsilon_{\text{stop}} \|\mathcal{C}\|_\infty + 2\eta \varepsilon_{\text{stop}} \log \left(\frac{1}{\varepsilon_{\text{stop}}} \left(\left(\prod_{k=1}^m n_k \right) - 1 \right) \right).$$

□

The following theorem demonstrates how the previous result can be combined with Algorithm 2 to obtain ε -accurate solutions.

Theorem 3. *Following the notation in Theorem 2, let $\hat{\mathcal{P}}$ be the tensor obtained by applying Algorithm 2 to $\tilde{\mathcal{P}}$. Let $\mathcal{P}^* = \arg \min_{P \in B(r_1, \dots, r_m)} \langle \mathcal{C}, \mathcal{P} \rangle$. Then it holds*

$$\langle \mathcal{C}, \hat{\mathcal{P}} \rangle - \langle \mathcal{C}, \mathcal{P}^* \rangle \leq \varepsilon,$$

where $\varepsilon = \varepsilon_{V_{\mathcal{C}}^\eta} + 2\eta \sum_{k=1}^m \log(n_k) + 2\varepsilon_{\text{stop}}$.

Proof. The tensor \mathcal{P}_η^* is the unique scaling of $\tilde{\mathcal{K}}$ with marginals r_1, \dots, r_m [4] and thus \mathcal{P}_η^* is also the unique minimizer [21] of

$$\arg \min_{P \in B(r_1, \dots, r_m)} \langle \mathcal{C}, \mathcal{P} \rangle - \eta H(\mathcal{P}).$$

In particular, $\langle \mathcal{C}, \mathcal{P}_\eta^* \rangle - \eta H(\mathcal{P}_\eta^*) \leq \langle \mathcal{C}, \mathcal{P}^* \rangle - \eta H(\mathcal{P}^*)$ and thus

$$\langle \mathcal{C}, \mathcal{P}_\eta^* \rangle - \langle \mathcal{C}, \mathcal{P}^* \rangle \leq \eta H(\mathcal{P}_\eta^*) - \eta H(\mathcal{P}^*) \leq \eta \sum_{k=1}^m \log(n_k), \quad (15)$$

where we use that $0 \leq H(\mathcal{X}) \leq \sum_{k=1}^m \log(n_k)$ for any tensor $\mathcal{C} \in \mathbb{R}^{n_1 \times \dots \times n_m}$ [13, Chapter 2]. Following the same argument, we have $V_{\mathcal{C}}^\eta(\mathcal{P}_\eta^*) \leq V_{\mathcal{C}}^\eta(\tilde{\mathcal{P}})$, which yields in combination with (9) that

$$\langle \mathcal{C}, \tilde{\mathcal{P}} \rangle - \langle \mathcal{C}, \mathcal{P}_\eta^* \rangle \leq \varepsilon_{V_{\mathcal{C}}^\eta} + \eta H(\tilde{\mathcal{P}}) - \eta H(\mathcal{P}_\eta^*) \leq \varepsilon_{V_{\mathcal{C}}^\eta} + \eta \sum_{k=1}^m \log(n_k). \quad (16)$$

Additionally, Lemma 1 yields

$$\langle \mathcal{C}, \hat{\mathcal{P}} \rangle - \langle \mathcal{C}, \tilde{\mathcal{P}} \rangle \leq \|\mathcal{C}\|_\infty \|\hat{\mathcal{P}} - \tilde{\mathcal{P}}\|_1 \leq 2\|\mathcal{C}\|_\infty \sum_{k=1}^m \varepsilon_{\text{stop}}. \quad (17)$$

By adding the Inequalities (15)-(17) we obtain

$$\langle \mathcal{C}, \hat{\mathcal{P}} \rangle - \langle \mathcal{C}, \mathcal{P}^* \rangle \leq \varepsilon_{V_{\mathcal{C}}^\eta} + 2\eta \sum_{k=1}^m \log(n_k) + 2 \sum_{k=1}^m \varepsilon_{\text{stop}}.$$

□

Note that for any $\varepsilon > 0$, we can find suitable $\eta, \varepsilon_{\log}, \varepsilon_{\text{stop}}$ such that combining Algorithm 3 and Algorithm 2 yields an ε -accurate solution for the multi-marginal optimal transport problem (1).

4 Tensor networks and graphical models

In applications, the cost tensor $\mathcal{C} \in \mathbb{R}_+^{n_1 \times \dots \times n_m}$ usually carries additional structure. A broad class of structures can be defined via graphical models [25]. In this case, the entries of \mathcal{C} takes the form

$$\mathcal{C}_I = \sum_{\alpha \in F} \mathcal{C}_{I_\alpha}^\alpha \quad \text{for every } I = (i_1, \dots, i_m), \quad 1 \leq i_k \leq n_k, \quad 1 \leq k \leq m, \quad (18)$$

where the summation indices $\alpha = (\alpha_1, \dots, \alpha_M)$ are contained in a fixed subset F of the power set of $\{1, \dots, m\}$, $I_\alpha := (i_{\alpha_1}, \dots, i_{\alpha_M})$, and $\mathcal{C}^\alpha \in \mathbb{R}_+^{n_{\alpha_1} \times \dots \times n_{\alpha_M}}$. The corresponding Gibbs kernel is given by a graphical model of the form

$$\mathcal{K}_I = \prod_{\alpha \in F} \mathcal{K}_{I_\alpha}^\alpha \quad \text{for every } I = (i_1, \dots, i_m), \quad 1 \leq i_k \leq n_k, \quad 1 \leq k \leq m, \quad (19)$$

where $\mathcal{K}^\alpha = \exp(-\mathcal{C}^\alpha/\eta)$. The topological structure of this product is a hypergraph with nodes $1, \dots, m$, hyperedges \mathcal{K}^α and all possible loops, i.e., edges from each node to itself. The dual of this hypergraph yields a tensor network [41] given by a hypergraph with vertices \mathcal{K}^α and $1, \dots, m$. This hypergraph can be transformed into a classical tensor network [35] by introducing identity tensor vertices and open edges. See Figure 1 for an example.

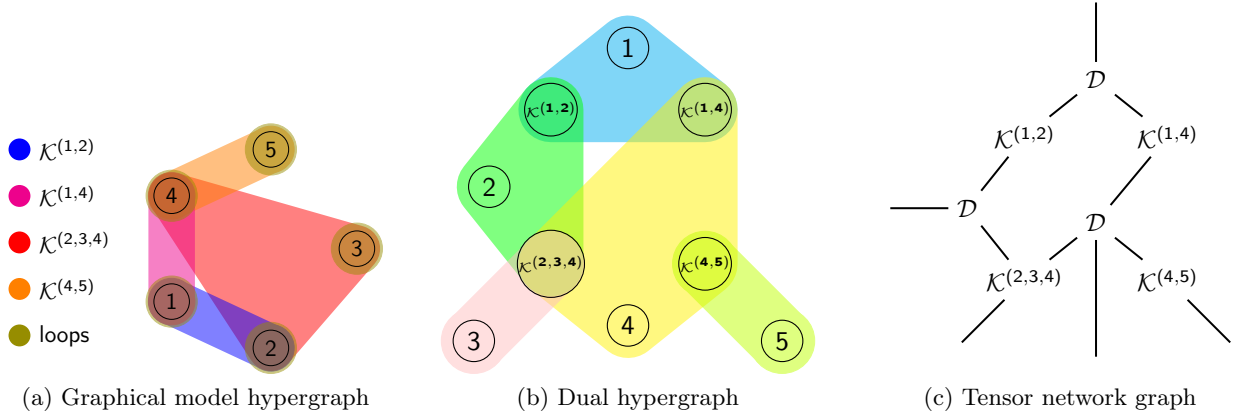


Figure 1: Example for a cost tensor $\mathcal{C} \in R_+^{n \times n \times n \times n \times n}$ given as in (18) by tensors $\mathcal{C}^{(1,2,3)}, \mathcal{C}^{(2,4)}, \mathcal{C}^{(3,4)}, \mathcal{C}^{(4,5)}$. We depict the hypergraph of the corresponding graphical model, its dual and a tensor network formulation of the dual, where we replaced hyperedges by introducing tensors \mathcal{D} of suitable order d and entries $\mathcal{D}_{i_1, \dots, i_d} = \delta_{i_1 i_2} \dots \delta_{i_{d-1} i_d}$, where δ denotes the Kronecker delta. In the hypergraphs edges are visualized using color. In the tensor network graph each open edge corresponds to one mode of the tensor.

In Algorithm 1, we need to evaluate the marginals of $\mathcal{P}_\eta^{(t)}$ in each iteration. Given a tensor network representation of \mathcal{K} , the mode- k marginals can be written as a contraction of the network [35] after connecting the matrix $\text{diag}(\beta_k)$ to the open edge corresponding to mode k , and the vectors $\beta_{\tilde{k}}$ for $\tilde{k} \neq k$ to their respective open edges. By contracting all inner edges of the resulting network, we obtain $r_k(\mathcal{P}_\eta^{(t)})$. We refer to Figure 2 for examples. Note that the structures of the tensor networks in (b) and (c) are reminiscent of the tensor train [36] and the hierarchical Tucker format [23].

We give a brief example on how to efficiently contract the network depicted in Figure 2(b). For the complexity analysis we assume $n_1 = n_2 = n_3 = n_4 = n$. Contracting β_1 and $\mathcal{K}^{(1,2)}$ can be performed in $n(2n - 1)$ operations each. Contracting the resulting vector \mathcal{D} , β_2 and $\mathcal{K}^{(2,3)}$ can be performed simultaneously exploiting the structure of \mathcal{D} in $n(3n - 1)$ operations. We obtain a second partial contraction by contracting $\mathcal{K}^{(3,4)}$ and β_4 in $n(2n - 1)$ operations. The final contraction of the two partial contractions, \mathcal{D} and $\text{diag}(\beta_3)$ can again be performed simultaneously exploiting the

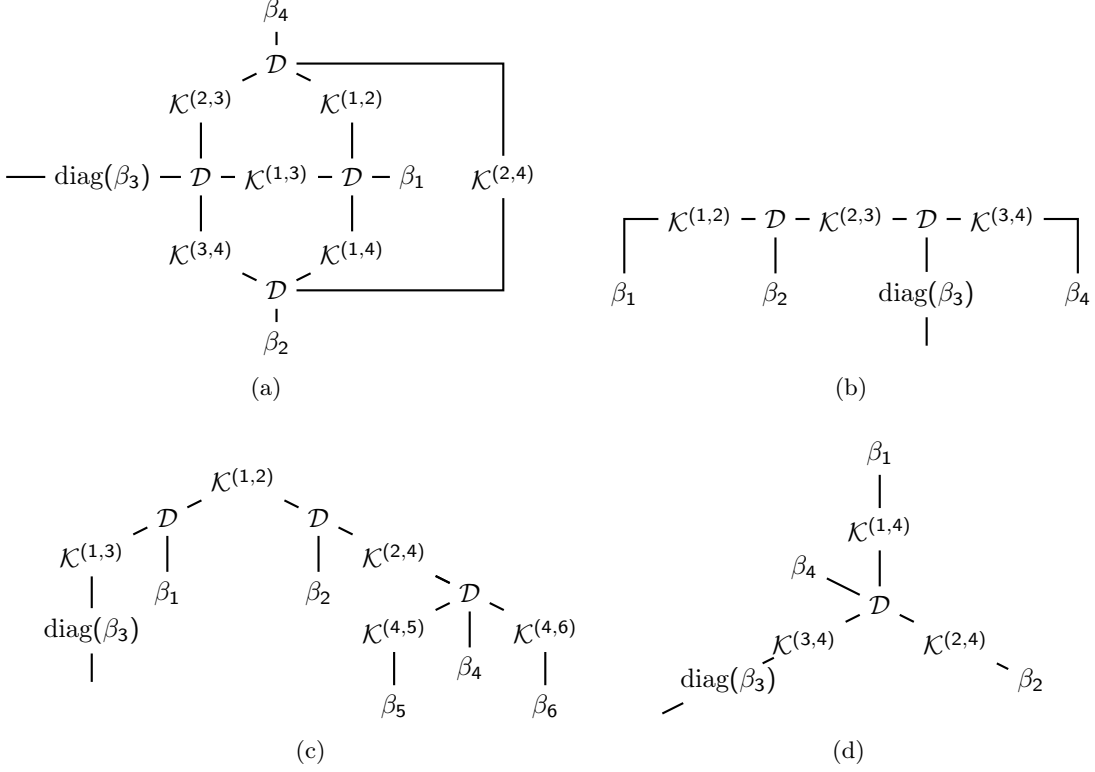


Figure 2: Examples for the tensor network diagram representation of $r_3(\mathcal{P}_\eta^{(t)})$ based on different graphical models (19): (a) fully connected graph, (b) line graph, (c) tree, (d) star graph. The tensors \mathcal{D} of suitable order d are defined as $\mathcal{D}_{i_1, \dots, i_d} = \delta_{i_1 i_2} \cdots \delta_{i_{d-1} i_d}$, where δ denotes the Kronecker delta.

structure in $3n$ operations. By reusing partial contractions, we can compute $r_k(\mathcal{P}_\eta^{(t)})$ for $k = 1, 2, 3, 4$ in only $16n^2 + 4n$ operations, whereas contractions based on the full tensor require $\mathcal{O}(n^4)$ operations.

5 Low-rank approximations in tensor networks.

Assuming that the Gibbs kernel is represented by a graphical model (19), we obtain a tensor network containing the coefficient tensors \mathcal{K}^α . The following lemma bounds the error when replacing each \mathcal{K}^α by an approximation $\tilde{\mathcal{K}}^\alpha$.

Lemma 2. Let $F \subset \{1, \dots, m\}^M$. Consider tensors $\mathcal{K}^\alpha \in \mathbb{R}_{>0}^{n_{\alpha_1} \times \dots \times n_{\alpha_M}}$ and $\tilde{\mathcal{K}}^\alpha \in \mathbb{R}_{>0}^{n_{\alpha_1} \times \dots \times n_{\alpha_M}}$ for every $\alpha = (\alpha_1, \dots, \alpha_M) \in F$. Define

$$\mathcal{K}_{i_1, \dots, i_m} = \prod_{\alpha \in F} \mathcal{K}_{I_\alpha}^\alpha, \quad \tilde{\mathcal{K}}_{i_1, \dots, i_m} = \prod_{\alpha \in F} \tilde{\mathcal{K}}_{I_\alpha}^\alpha. \quad (20)$$

Then

$$\|\log(\mathcal{K}) - \log(\tilde{\mathcal{K}})\|_\infty \leq \sum_{\alpha \in F} \|\log(\mathcal{K}^\alpha) - \log(\tilde{\mathcal{K}}^\alpha)\|_\infty.$$

Proof.

$$\begin{aligned}
\|\log(\mathcal{K}) - \log(\tilde{\mathcal{K}})\|_\infty &= \max_{i_1, \dots, i_m} \left| \sum_{\alpha \in F} \log(\mathcal{K}_{I_\alpha}^\alpha) - \sum_{\alpha \in F} \log(\tilde{\mathcal{K}}_{I_\alpha}^\alpha) \right| \\
&\leq \max_{i_1, \dots, i_m} \sum_{\alpha \in F} |\log(\mathcal{K}_{I_\alpha}^\alpha) - \log(\tilde{\mathcal{K}}_{I_\alpha}^\alpha)| \\
&\leq \sum_{\alpha \in F} \|\log(\mathcal{K}^\alpha) - \log(\tilde{\mathcal{K}}^\alpha)\|_\infty
\end{aligned}$$

□

Combining Lemma 2 and Theorem 2 implies that Algorithm 3 with $\tilde{\mathcal{K}}$ defined as in (20) yields an accurate approximation of the optimal transport plan when $\|\log(\mathcal{K}^\alpha) - \log(\tilde{\mathcal{K}}^\alpha)\|_\infty$ is sufficiently small for all $\alpha \in F$. This allows one to replace each \mathcal{K}^α by a low-rank approximation $\tilde{\mathcal{K}}^\alpha$, which in turn accelerates the computation of tensor network contractions. For the example at the end of Section 4, the number of operations reduces from $\mathcal{O}(n^2)$ to $\mathcal{O}(nr)$ when every \mathcal{K}^α is approximated by a rank- r matrix of the form $\mathcal{K}^\alpha = U^\alpha (V^\alpha)^T$ with $U^\alpha, V^\alpha \in \mathbb{R}^{n \times r}$ as depicted in Figure 3(a).

6 Numerical Experiments

All numerical experiments in this section were performed in MATLAB R2018b on a Lenovo Thinkpad T480s with Intel Core i7-8650U CPU and 15.4 GiB RAM. The code to reproduce these results is available from <https://github.com/cstroessner/Optimal-Transport.git>.

6.1 Proof of concept

In the following, we use the example in Section 4.6 in [3] to study the impact of approximating the Gibbs kernel on the transport cost. Let $X^{(1)}, X^{(2)}, X^{(3)}, X^{(4)}$ denote sets each containing $n = 420$ points sampled uniformly from $[0, 1]^2$. We define $n \times n$ matrices $C^{(1,2)}, C^{(2,3)}, C^{(3,4)}$ with entries

$$\mathcal{C}_{i,j}^{(1,2)} = \|x_i^{(1)} - x_j^{(2)}\|_2^2, \quad \mathcal{C}_{j,k}^{(2,3)} = \|x_j^{(2)} - x_k^{(3)}\|_2^2, \quad \mathcal{C}_{k,l}^{(3,4)} = \|x_k^{(3)} - x_l^{(4)}\|_2^2 \quad \text{for } 1 \leq i, j, k, l \leq n,$$

where $\|\cdot\|_2$ denotes the Euclidean norm. We construct the cost tensor

$$\mathcal{C}_{i,j,k,l} = \mathcal{C}_{i,j}^{(1,2)} + \mathcal{C}_{j,k}^{(2,3)} + \mathcal{C}_{k,l}^{(3,4)} \quad \text{for } 1 \leq i, j, k, l \leq n.$$

Let $\mathcal{K}^\alpha = \exp(-\mathcal{C}^\alpha)$ for $\alpha \in \{(1,2), (2,3), (3,4)\}$. Then the Gibbs kernel $\mathcal{K} = \exp(-\mathcal{C})$ has the line graph structure shown in Figure 2(b).

Let $r \leq n$. We compare two different approximations of \mathcal{K} . For the first one, we replace the matrices \mathcal{K}^α by their rank- r best approximations $\tilde{\mathcal{K}}^\alpha$ using truncated singular value decompositions (SVDs) and define

$$(\mathcal{K}_{\text{SVDs}})_{i,j,k,l} = \tilde{\mathcal{K}}_{i,j}^{(1,2)} \cdot \tilde{\mathcal{K}}_{j,k}^{(2,3)} \cdot \tilde{\mathcal{K}}_{k,l}^{(3,4)} \quad \text{for } 1 \leq i, j, k, l \leq n.$$

For the second approximation \mathcal{K}_{TT} , we compute a tensor train (TT) approximation [36] of \mathcal{K} with ranks (r, r, r, r) using the TT-DMRG-cross algorithm [42] ignoring the underlying graphical model. The tensor network representation of $\mathcal{K}_{\text{SVDs}}$ and \mathcal{K}_{TT} is depicted in Figure 3. All four marginals

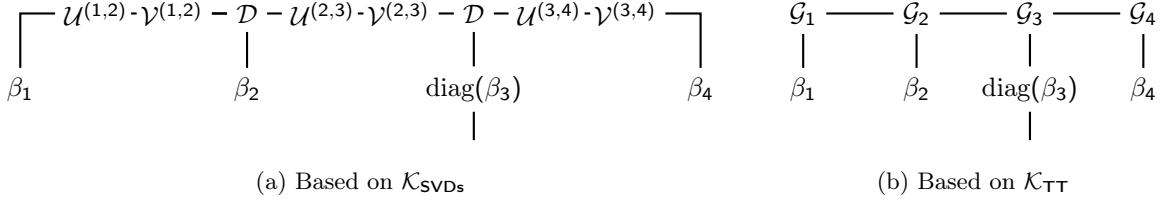


Figure 3: Tensor networks for the computation of $r_3(\mathcal{P}_\eta^{(t)})$ for the example in Section 6.1. We express the truncated SVDs in $\mathcal{K}_{\text{SVDs}}$ as $\tilde{\mathcal{K}}^\alpha = U^\alpha (V^\alpha)^T$ with $U^\alpha, V^\alpha \in \mathbb{R}^{n \times r}$. The TT cores in \mathcal{K}_{TT} are denoted by $\mathcal{G}_1 \in \mathbb{R}^{n \times r}$, $\mathcal{G}_2, \mathcal{G}_3 \in \mathbb{R}^{r \times n \times r}$ and $\mathcal{G}_4 \in \mathbb{R}^{r \times n}$.

can be computed in $\mathcal{O}(nr)$ operations for $\mathcal{K}_{\text{SVDs}}$ and in $\mathcal{O}(nr^2)$ operations for \mathcal{K}_{TT} by contracting the tensor networks. In contrast, exploiting the graphical model without low-rank approximations requires $\mathcal{O}(n^2)$ operations.

Based on the tensors $\mathcal{K}, \mathcal{K}_{\text{SVDs}}, \mathcal{K}_{\text{TT}}$, we compute transport plans $\mathcal{P}, \mathcal{P}_{\text{SVDs}}, \mathcal{P}_{\text{TT}}$ by first applying Algorithm 3 with marginals $r_k = \frac{1}{n_k} \cdot \mathbf{1}_{n_k}$, index selection (7), stopping criterion (8) where $\varepsilon_{\text{stop}} = 10^{-4}$ and then rounding the resulting tensor using Algorithm 2. In Figure 4, we compare the different transport plans. Note that we can efficiently evaluate the transport cost $\langle \mathcal{C}, \mathcal{P} \rangle$ using tensor network contractions of \mathcal{C}^α and \mathcal{P} without evaluating the full tensors. We observe that the difference in transport cost of $\mathcal{P}_{\text{SVDs}}, \mathcal{P}_{\text{TT}}$ and \mathcal{P} is much smaller than the norm of the difference of the logarithms of $\mathcal{K}_{\text{SVDs}}, \mathcal{K}_{\text{TT}}$ and \mathcal{K} , i.e. the bound in Theorem 2 is not sharp. The approximation $\mathcal{P}_{\text{SVDs}}$ which exploits the graphical model leads to slightly better approximations compared to \mathcal{P}_{TT} . We want to emphasize that computing $\mathcal{P}_{\text{SVDs}}$ with $r = 25$ is faster than using the graphical model of \mathcal{K} directly and only leads to a difference in transport cost in the order of machine precision. Computing \mathcal{P}_{TT} is faster than computing \mathcal{P} for very small ranks, but the computational time increases more for larger r compared to $\mathcal{P}_{\text{SVDs}}$.

Remark. The most expensive step in the computation of $\mathcal{P}_{\text{SVDs}}$ is the computation of the low-rank approximations using the truncated SVD. There exist cheaper algorithms for approximating \mathcal{K}^α including the adaptive cross approximation [5] and the randomized SVD [26].

6.2 Application: Color transfer

In the following, we apply our algorithms for color transfer as in [25]. We consider $k = 4$ images containing $n = 100^2$ pixels each. Let $0 \leq \lambda_1, \lambda_2, \lambda_3$ such that $\lambda_1 + \lambda_2 + \lambda_3 = 1$. Our goal is to transfer the color of the first three images weighted by $\lambda = (\lambda_1, \lambda_2, \lambda_3)$ onto the fourth image, which can be expressed as multi-marginal optimal transport problem.

Let $x_i^{(k)} \in [0, 1]^3$ denote the color of pixel i in image k , where we treat the RGB values as element in \mathbb{R}^3 and rescale to $[0, 1]^3$. Let $\mathcal{C}_{i,j}^{(k_1,k_2)} = \|x_i^{(k_1)} - x_j^{(k_2)}\|_2^2$ for $1 \leq i, j \leq n$ and $\mathcal{K}^{(k_1,k_2)} = \exp(-\mathcal{C}^{(k_1,k_2)}/\eta)$ for $1 \leq k_1, k_2 \leq k$. We define the cost tensor

$$\mathcal{C}_{i,j,k,l} = \lambda_1 \mathcal{C}_{i,l}^{(1,4)} + \lambda_2 \mathcal{C}_{j,l}^{(2,4)} + \lambda_3 \mathcal{C}_{k,l}^{(3,4)} \quad \text{for } 1 \leq i, j, k, l \leq n.$$

From the solution \mathcal{P} of the problem (2) with cost tensor \mathcal{C} and marginals $r_k = \mathbf{1}$, we compute the

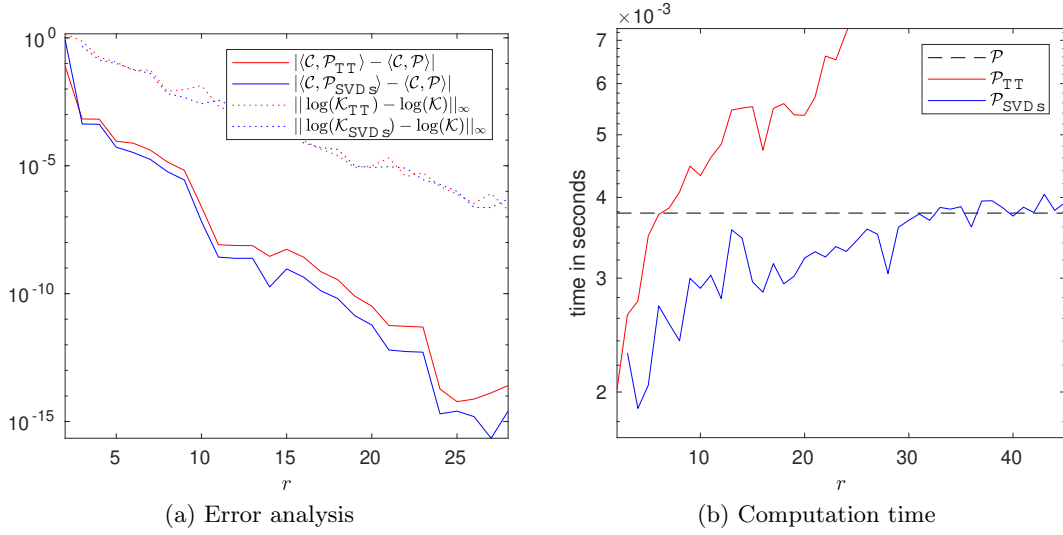


Figure 4: Difference in transport cost for the example in Section 6.1 for various ranks r . Left: We depict the difference in transport cost for $\mathcal{P}_{\text{SVDs}}$, \mathcal{P}_{TT} and \mathcal{P} and an estimation of the norm of the difference of the logarithms of $\mathcal{K}_{\text{SVDs}}$, \mathcal{K}_{TT} and \mathcal{K} based on 1000 sample points. Right: Measured computation times for applying Algorithm 3 and 2 to compute the transport plans exploiting the structures of \mathcal{K} , $\mathcal{K}_{\text{SVDs}}$, \mathcal{K}_{TT} .

color vector of the target image with transferred colors as

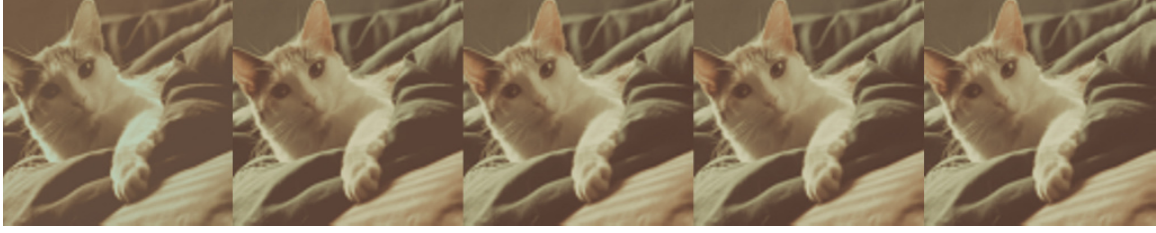
$$x_l^* = \sum_{i=1}^n \sum_{j=1}^n \sum_{k=1}^n \mathcal{P}_{i,j,k,l} (\lambda_1 x_i^{(1)} + \lambda_2 x_j^{(2)} + \lambda_3 x_k^{(3)}) \quad \text{for } 1 \leq l \leq n. \quad (21)$$

The resulting Gibbs kernel $\mathcal{K} = \exp(-\mathcal{C}/\eta)$ corresponds to a star shaped graphical model build from $\mathcal{K}^\alpha = \exp(-\mathcal{C}^\alpha/\eta)$ as in Figure 2(d). To accelerate the computation of marginals, we replace the tensors \mathcal{K}^α by rank- r approximations $\tilde{\mathcal{K}}^\alpha$ for $\alpha \in \{(1,4), (2,4), (3,4)\}$ using the randomized SVD [26]. Marginals can now be computed in $\mathcal{O}(nr)$ operations. We set $\eta = 1/10$ and compute approximate transport plans $\tilde{\mathcal{P}}$ by applying Algorithm 3 and 2 as in Section 6.1. Using the structure of $\tilde{\mathcal{P}}$, we can compute the resulting image, defined analogously as in Equation (21), as sum of tensor network contractions in $\mathcal{O}(nr)$ operations.

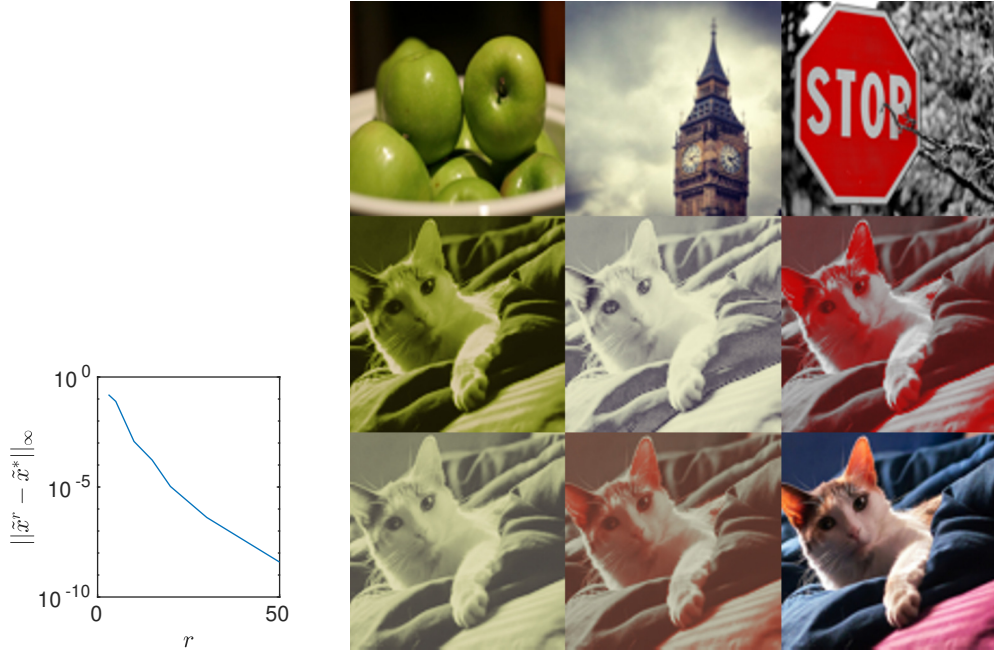
In Figure 5, we study the impact of λ and r onto the color transferred image for example images from the COCO data set [33]. We observe that small values of r suffice to accurately approximate the desired image. The computation including the assembling of the matrices and the randomized SVD takes 1.29 seconds for $r = 50$, whereas using the matrices $\mathcal{K}^\alpha \in \mathbb{R}^{10000 \times 10000}$ directly in the tensor network takes 41.6 seconds, i.e. our low-rank approach reduces the computation time by over 96%.

7 Conclusion

Multi-marginal optimal transport problems can be solved using the multi-marginal Sinkhorn algorithm, which suffers from the curse of dimensionality unless marginals can be computed efficiently.



(a) Impact of r



(b) Error decay

(c) Impact of λ

Figure 5: Given the images displayed in the top row of (c), we use the method described in Section 6.2 to transfer their color to the bottom right image in (c). For fixed $\lambda = (1/3, 1/3, 1/3)$, we plot the resulting images for $r = 3, r = 5, r = 10, r = 50$ from left to right in (a). The rightmost picture is obtained by using the full matrices \mathcal{K}^α directly. In (b), we plot $\|\tilde{x}^r - \tilde{x}^*\|_\infty$ where \tilde{x}^r denotes the resulting image vector for a given r and \tilde{x}^* is computed using the full matrices \mathcal{K}^α directly. Moreover, we display the resulting image for different values of λ in (c): middle row left to right $\lambda = (1, 0, 0)$, $\lambda = (0, 1, 0)$, $\lambda = (0, 0, 1)$, bottom row left $\lambda = (1/3, 2/3, 0)$, bottom row middle $\lambda = (1/5, 1/5, 3/5)$.

In this paper, we analyze how approximations of the Gibbs kernel, which potentially drastically reduce the complexity of computing marginals, affect the solution of the transport problem. We demonstrate that computing marginals for Gibbs kernels based on graphical models can be accelerated by introducing low-rank approximations in their dual tensor network. We show that this approach can be faster and more accurate than direct low-rank approximations of the full Gibbs kernel. An application of our method is presented by the drastic reduction of the computation time for transferring colors from several images onto one target image.

In other applications, there are, however, are several obstacles to put this into practice. For

instance, in density functional theory, the Coulomb cost leads to zero entries on the diagonal of the Gibbs kernel. Any approximation of the Gibbs kernel would need to approximate these entries exactly, which is not feasible without adding a sparse correction term to the low-rank approximations. Moreover, the full graph in the underlying graphical model leads to a tensor network, which can not be contracted efficiently. In future work, the use of non-negative low-rank approximations could be of interest.

References

- [1] J. ALTSCHULER, F. BACH, A. RUDI, AND J. NILES-WEED, *Massively scalable Sinkhorn distances via the Nyström method*, in Adv. Neural Inf. Process. Syst. 32, 2019, p. 4427–4437.
- [2] J. ALTSCHULER, J. WEED, AND P. RIGOLLET, *Near-linear time approximation algorithms for optimal transport via Sinkhorn iteration*, in Adv. Neural Inf. Process. Syst. 30, 2017, pp. 1964–1974.
- [3] J. M. ALTSCHULER AND E. BOIX-ADSERÀ, *Polynomial-time algorithms for multimarginal optimal transport problems with structure*, arXiv e-prints, (2020), p. arXiv:2008.03006.
- [4] R. BAPAT, *D_1AD_2 theorems for multidimensional matrices*, Linear Algebra Appl., 48 (1982), pp. 437–442.
- [5] M. BEBENDORF, *Approximation of boundary element matrices*, Numer. Math., 86 (2000), pp. 565–589.
- [6] F. BEIER, J. VON LINDHEIM, S. NEUMAYER, AND G. STEIDL, *Unbalanced multi-marginal optimal transport*, arXiv e-prints, (2021), p. arXiv:2103.10854.
- [7] J.-D. BENAMOU, *Optimal transportation, modelling and numerical simulation*, Acta Numer., 30 (2021), pp. 249–325.
- [8] J.-D. BENAMOU, G. CARLIER, M. CUTURI, L. NENNA, AND G. PEYRÉ, *Iterative Bregman projections for regularized transportation problems*, SIAM J. Sci. Comput., 37 (2015), pp. A1111–A1138.
- [9] J.-D. BENAMOU, G. CARLIER, AND L. NENNA, *Generalized incompressible flows, multi-marginal transport and Sinkhorn algorithm*, Numer. Math., 142 (2019), pp. 33–54.
- [10] J. CAO, L. MO, Y. ZHANG, K. JIA, C. SHEN, AND M. TAN, *Multi-marginal wasserstein GAN*, in Adv. Neural Inf. Process. Syst. 32, 2019, pp. 1776–1786.
- [11] G. CARLIER, *On the linear convergence of the multi-marginal Sinkhorn algorithm*. hal-03176512, 2021.
- [12] G. CARLIER, A. OBERMAN, AND E. OUDET, *Numerical methods for matching for teams and Wasserstein barycenters*, ESAIM Math. Model. Numer. Anal., 49 (2015), pp. 1621–1642.
- [13] T. M. COVER AND J. A. THOMAS, *Elements of information theory*, Wiley-Interscience [John Wiley & Sons], Hoboken, NJ, second ed., 2006.
- [14] M. CUTURI, *Sinkhorn distances: Lightspeed computation of optimal transport*, in Adv. Neural Inf. Process. Syst. 26, 2013, pp. 2292–2300.
- [15] S. DI MARINO, A. GEROLIN, AND L. NENNA, *Optimal transportation theory with repulsive costs*, in Topological optimization and optimal transport, vol. 17 of Radon Ser. Comput. Appl. Math., De Gruyter, Berlin, 2017, pp. 204–256.
- [16] P. DVURECHENSKY, A. GASNIKOV, AND A. KROSHNIN, *Computational optimal transport: Complexity by accelerated gradient descent is better than by Sinkhorn’s algorithm*, in 35th Int. Conf. Mach. Learn., 2018, pp. 1367–1376.
- [17] F. ELVANDER, I. HAASLER, A. JAKOBSSON, AND J. KARLSSON, *Multi-marginal optimal transport using partial information with applications in robust localization and sensor fusion*, Signal Process., 171 (2020), p. 107474.

- [18] J. FAN, I. HAASLER, J. KARLSSON, AND Y. CHEN, *On the complexity of the optimal transport problem with graph-structured cost*, arXiv e-prints, (2021), p. arXiv:2110.00627.
- [19] J. FEYDY, B. CHARLIER, F.-X. VIALARD, AND G. PEYRÉ, *Optimal transport for diffeomorphic registration*, in MICCAI, 2017, pp. 291–299.
- [20] J. FRANKLIN AND J. LORENZ, *On the scaling of multidimensional matrices*, Linear Algebra Appl., 114/115 (1989), pp. 717–735.
- [21] S. FRIEDLAND, *Tensor optimal transport, distance between sets of measures and tensor scaling*, arXiv e-prints, (2020), p. arXiv:2005.00945.
- [22] A. GENEVAY, G. PEYRE, AND M. CUTURI, *Learning generative models with sinkhorn divergences*, in Int. Conf. Artif. Intell. Stat., 2018, pp. 1608–1617.
- [23] L. GRASEDYCK, D. KRESSNER, AND C. TOBLER, *A literature survey of low-rank tensor approximation techniques*, GAMM-Mitt., 36 (2013), pp. 53–78.
- [24] I. HAASLER, A. RINGH, Y. CHEN, AND J. KARLSSON, *Multimarginal optimal transport with a tree-structured cost and the Schrödinger bridge problem*, SIAM J. Control Optim., 59 (2021), pp. 2428–2453.
- [25] I. HAASLER, R. SINGH, Q. ZHANG, J. KARLSSON, AND Y. CHEN, *Multi-marginal optimal transport and probabilistic graphical models*, IEEE Trans. Inf. Theory, 67 (2021), pp. 4647–4668.
- [26] N. HALKO, P. G. MARTINSSON, AND J. A. TROPP, *Finding structure with randomness: probabilistic algorithms for constructing approximate matrix decompositions*, SIAM Rev., 53 (2011), pp. 217–288.
- [27] S.-W. HO AND R. W. YEUNG, *The interplay between entropy and variational distance*, IEEE Trans. Inform. Theory, 56 (2010), pp. 5906–5929.
- [28] H. A. L. KIERS, *Towards a standardized notation and terminology in multiway analysis*, Journal of Chemometrics, 14 (2000), pp. 105–122.
- [29] T. G. KOLDA AND B. W. BADER, *Tensor decompositions and applications*, SIAM Rev., 51 (2009), pp. 455–500.
- [30] S. KOLOURI, S. R. PARK, M. THORPE, D. SLEPCEV, AND G. K. ROHDE, *Optimal mass transport: Signal processing and machine-learning applications*, IEEE Signal Process. Mag., 34 (2017), pp. 43–59.
- [31] T. LIN, N. HO, M. CUTURI, AND M. I. JORDAN, *On the complexity of approximating multimarginal optimal transport*, arXiv e-prints, (2019), p. arXiv:1910.00152.
- [32] T. LIN, N. HO, AND M. I. JORDAN, *On efficient optimal transport: An analysis of greedy and accelerated mirror descent algorithms*, in 36th Int. Conf. Mach. Learn., 2019, pp. 3982–3991.
- [33] T.-Y. LIN, M. MAIRE, S. BELONGIE, J. HAYS, P. PERONA, D. RAMANAN, P. DOLLÁR, AND C. L. ZITNICK, *Microsoft COCO: Common objects in context*, in ECCV, 2014, pp. 740–755.
- [34] M. MOZAFFARI, W. SAAD, M. BENNIS, AND M. DEBBAH, *Optimal transport theory for power-efficient deployment of unmanned aerial vehicles*, in IEEE Int. Conf. Commun., 2016, pp. 1–6.
- [35] R. ORÚS, *A practical introduction to tensor networks: matrix product states and projected entangled pair states*, Ann. Physics, 349 (2014), pp. 117–158.
- [36] I. V. OSELEDETS, *Tensor-train decomposition*, SIAM J. Sci. Comput., 33 (2011), pp. 2295–2317.
- [37] B. PASS, *Multi-marginal optimal transport: Theory and applications*, ESAIM: M2AN, 49 (2015), pp. 1771–1790.
- [38] G. PEYRÉ AND M. CUTURI, *Computational Optimal Transport: With Applications to Data Science*, now, 2019.
- [39] J. RABIN, S. FERRADANS, AND N. PAPADAKIS, *Adaptive color transfer with relaxed optimal transport*, in IEEE Int. Conf. Imag. Process., 2014, pp. 4852–4856.

- [40] S.-J. RAN, E. TIRRITO, C. PENG, X. CHEN, L. TAGLIACCOZZO, G. SU, AND M. LEWENSTEIN, *Tensor Network Contractions: Methods and Applications to Quantum Many-Body Systems*, vol. 964 of Lecture Notes in Physics, Springer International Publishing, Cham, 2020.
- [41] E. ROBEVA AND A. SEIGAL, *Duality of graphical models and tensor networks*, Inf. Inference, 8 (2019), pp. 273–288.
- [42] D. SAVOSTYANOV AND I. OSELEDETS, *Fast adaptive interpolation of multi-dimensional arrays in tensor train format*, in 7th Int. Workshop Multidimens. (nD) Syst., 2011, pp. 1–8.
- [43] M. SCETBON, M. CUTURI, AND G. PEYRÉ, *Low-rank Sinkhorn factorization*, arXiv e-prints, (2021), p. arXiv:2103.04737.
- [44] R. SINKHORN, *A relationship between arbitrary positive matrices and doubly stochastic matrices*, Ann. Math. Statist., 35 (1964), pp. 876–879.
- [45] A. THIBAUT, L. CHIZAT, C. DOSSAL, AND N. PAPADAKIS, *Overrelaxed Sinkhorn-Knopp algorithm for regularized optimal transport*, Algorithms, 14 (2021). Paper No. 143.
- [46] C. VILLANI, *Optimal Transport: Old and New*, Grundlehren der mathematischen Wissenschaften, Springer, 1st ed., 2009.